RSC Advances

ROYAL SOCIETY OF CHEMISTRY

www.rsc.org/advances

The Enhanced Electrocaloric Effect in P(VDF-TrFE) Copolymer with Barium Strontium Titanate Nano-fillers Synthesized via an Effective Hydrothermal Method

Z. Y. Jiang[1], X. C. Zheng[1,2*], and G. P. Zheng[1*]

[1] Department of Mechanical Engineering, The Hong Kong Polytechnic University, Hung Hom, Kowloon, Hong Kong, China
[2] College of Chemistry and Molecular Engineering, Zhengzhou University, Zhengzhou 450001, China
*Corresponding authors. E-mail: mmzheng@polyu.edu.hk (GP Zheng); zhxch@zzu.edu.cn (XC Zheng)

Abstract

An effective hydrothermal method is developed to synthesize barium strontium titanate (BST) nanoparticles with a mean size below 30 nm, which are used for the fabrication of nanocomposite films consisting of ferroelectric co-polymer poly(vinylidene fluoride-trifluoroethylene) (P(VDF-TrFE)) and the ceramic nanoparticles. The interface between the nanoparticle and the polymeric matrix is found to improve the polarization and pyroelectric behaviors of the nanocomposites, resulting in much enhanced electrocaloric effect as compared with that of the pristine P(VDF-TrFE). The electrocaloric temperature change is 2.5 ºC under electric fields of ~600 kV/cm. The effects of $Ba_{0.75}Sr_{0.25}TiO_3$ nanoparticles on the ferroelectric-to-paraelectric transition of P(VDF-TrFE) are investigated using dynamical mechanical relaxation. The results suggest that the improved electrocaloric effect in the nanocomposites could be related with the localized polarization field near the surfaces of $Ba_{0.75}Sr_{0.25}TiO_3$ nanoparticles.

Keywords: Electrocaloric effect; Nanocomposites; Thermal analysis; Hydrothermal

1. Introduction

Under an applied electric field the entropy of a ferroelectric material changes with the ordering of dipoles, resulting in the electrocaloric effect (ECE). The ECE is promising in solid-state refrigeration especially in the cooling of electronic devices because of the high energy efficiency and small sizes of the ferroelectric refrigerants. It is an essential step in the implementation of this novel refrigeration technology that the ferroelectric refrigerants with giant ECE, i.e., refrigerants with refrigeration temperature change (ΔT) larger than 10 ^{o}C [1-2], are developed. Contrary to lead-based ferroelectric materials lead-free ferroelectric ceramics and polymers are environmental-friendly and have been pursued for EC cooling in the past decade [3]. For examples, multi-layered barium titanate based thin and thick films have been observed to exhibit a directly measured ΔT of 10 °C [4-7]; The giant ECE has been also found in poly(vinylidene fluoride) (PVDF) based co-polymer or ter-polymer thin films [8]. Both groups of lead-free materials have been well investigated with their pyroelectric and ferroelectric properties and the giant ECEs can be optimized to occur at ambient temperatures. The barium titanate based ceramics have an EC strength α (the ratio of ΔT to the change in the applied electric field ΔE) as large as 30 $K \cdot cm \cdot MV^{-1}$ while they cannot withstand high ΔE [6,9]. PVDF-based co- or ter-polymers can withstand ultra-high ΔE (~ 10 MV/cm) which is much large than that (<1 MV/cm) of barium titanate based ceramics but their EC strength is typically small (α~2 $K \cdot cm \cdot MV^{-1}$) [10]. PVDF-based co- or ter-polymer matrix composites containing barium titanate based ceramics are expected to have large EC strength and

withstand ultra-high ΔE [11,12]. Hence, these composites could be ideal lead-free ferroelectric refrigerants since they have giant ECE and they are flexible and easy to process.

In this work, we synthesize nanocomposites consisting of poly(vinylidene fluoride-trifluoroethylene) (P(VDF-TrFE)-52/48 mol%) and barium strontium titanate ($Ba_{0.75}Sr_{0.25}TiO_3$, BST) nano-particles and investigate their EC properties. Since the giant ECE is usually associated with ultra-high electric field applied to the nanocomposites, BST nanoparticles with uniform sizes and round shapes should be used to fabricate them. Otherwise the localized electric fields close to the interfaces may cause electrical breakdowns of the nanocomposites. In this work, fine spherical BST nanoparticles are synthesized with a facile hydrothermal method with common starting materials and an efficient routine.

The ferroelectric-to-paraelectric (FE-to-PE) transition temperatures of bulk P(VDF-TrFE)-52/48 mol% and $Ba_{0.75}Sr_{0.25}TiO_3$ where the maximum ECE occurs are similar with each other (~45-62 ^{o}C) [7,13]. In the nanocomposites the interface between nanoparticles and polymer matrix is an important factor which determines the ECE properties. In this work the effects of interfaces on the structural properties of the polymeric matrix and its FE-to-PE phase transition are characterized by mechanical relaxation and thermal analyses.

2. Experimental

2.1 Synthesis of materials

$Ba_{0.75}Sr_{0.25}TiO_3$ nanoparticles were synthesized via a facile hydrothermal method. Without using complex acids and $TiCl_4$ commonly used in the synthesis of BST [14,15], the starting materials of barium chloride dihyrate ($BaCl_2 \cdot 2H_2O$), strontium chloride hexahydrate ($SrCl_2 \cdot 6H_2O$) and chlorhydric acid (HCl) solution of 15.0% titanium trichloride ($TiCl_3$) are used in the hydrothermal process. Compared with other methods in the synthesis of BST, the hydrothermal method developed in this work is simple and efficient in preparing BST nanoparticles with sizes below 30 nm [14,15]. In brief, 24 mmol of $BaCl_2 \cdot 2H_2O$ and $SrCl_2 \cdot 6H_2O$ was dissolved with 20 mL of water at room temperature. Subsequently, 15 mmol of $TiCl_3$ solution was added and the system was stirred for 20 minutes. The initial precursor molar ratio of Ba and/or Sr to Ti was equal to 1.6. This ratio was proved to form $Ba_xSr_{1-x}TiO_3$ ($0 \leq x < 1$), which was similar to that in preparing $BaTiO_3$. 30 mL of NaOH solution (14.4 mol/L) was added under vigorous stirring and the solution was stirred for about 1.5 h. The obtained suspension was transferred into a 100 mL Teflon-lined stainless-steel autoclave and crystallized at 180 °C for 8 h. After cooling down to room temperature, the solution pH was adjusted to about 3.0 by adding 1.0 mol/L solution of HCl under stirring to dissolve the very little portion of $BaCO_3$ and $SrCO_3$. The precipitates were separated by centrifuging, washed with water, dried at 110 °C overnight to get white BST powders.

The BST powders were uniformly dispersed in N,N-dimethylformamide (DMF) and ultrasonicated for 0.5h to reduce agglomeration. The solution was mechanically stirred for 4h. Then co-polymer P(VDF-TrFE)-52/48 mol% (PiezoTech, France)

powders were added slowly under magnetic stirring at 70 °C till the co-polymer powders were dissolved in the solution. The mass ratio of BST to P(VDF-TrFE) is 26 %, corresponding to 10% volume ratio of BST nano-fillers to the P(VDF-TrFE) matrix. The solution was further stirred for 8h to allow uniformly mixing of co-polymer and BST nanoparticles. The solution was then casted on the surface of a flat copper foil with a thickness of ~0.01 mm to form film samples. The DMF in the film was evaporated in a drying oven at 70 °C and the film was further heat-treated at 110 °C in a vacuum oven for 12h. Finally the nanocomposite film with a thickness of 20-50 μm was formed on the surface of the copper foil.

2.2 Characterization methods

The X-ray diffractometer (Rigaku Smartlab) with the Cu Kα radiation (λ = 0.154 nm) sources operated at 45 kV and 200 mA was used to characterize the crystal structures of the materials. Scanning electron microscopy (Hitachi S4800) was utilized to observe the microstructures of the nanocomposites and the ceramic nanoparticles. The specific surface area of the BST powders was calculated from nitrogen adsorption isotherms at 77 K by the Brunauer-Emmett-Teller (BET) method. Prior to the measurements on the nitrogen adsorption isotherms using a surface area and porosity analyzer (Micromeritics ASAP 2420), the samples were degassed in vacuum at 250 °C for 2 h. The temperature-dependent P-E hysteresis loops were tested in a ferroelectric test system (TF2000, aixACCT). Silver paste layer with a thickness of 80 μm was covered on top surface of the nanocomposite film to form an electrode. The copper substrate of the film was used as another electrode. The dynamic mechanical analysis (DMA, TA Instruments Q800) in a tensile mode was used to characterize the mechanical relaxation of the free-standing film samples with dimensions of 10×5×0.02 mm^3. The heating rate is 0.2 °C/min. Thermal analyses were

performed in the differential scanning calorimeter (DSC, TA Instruments Q200) in conventional and temperature-modulated modes.

3. Results and discussion

3.1 Characterizations

Single-phase $Ba_{0.75}Sr_{0.25}TiO_3$ was successfully prepared by the facile hydrothermal method described above. The X-ray diffraction (XRD) patterns of BST are shown in Fig. 1(a). The mean size of BST nanoparticles determined from the Scherrer equation using the (110) diffraction peak is about d=27.5 nm, which is in good agreement with that measured from the SEM images (Fig. 2(a)). The BET specific surface area of the BST nanoparticles is 80 m^2/g, which is much larger than those of BST samples synthesized by other methods [16-19]. These results indicate that the BST nanoparticles are uniform and in spherical shape and could act as excellent nano-fillers in P(VDF-TrFE) co-polymer for ECE applications.

The XRD patterns of P(VDF-TrFE) and BST-P(VDF-TrFE) nanocomposites are shown in Fig. 1(a). The broad peak around 19^o indicates the co-existence of crystalline non-polar α and polar β phases of the copolymer, corresponding to the diffractions of {020} at 18.7^o and {110} at 19.2^o, respectively [20]. To further characterize the crystalline phases in P(VDF-TrFE) before and after the filling of BST nanoparticles, the peaks between 17.5^o and 20.5^o were analyzed, as shown in Fig. 1(b). The pristine P(VDF-TrFE) has a weak (110) peak of crystalline β phases relative to the (020) peak of α phase. The filling of BST nanoparticles in the P(VDF-TrFE)

matrix obviously enhances the polar β phases, manifesting by the relatively strong (110) peak and its position exactly at 19.2°. As second-phase fillers, BST nanoparticles are not likely to alternate the local compositions of VDF and TrFE in the polymer matrix. The enhanced ferroelectric β phase in P(VDF-TrFE) filled with BST nanoparticles implies that the BST nanoparticles still possess spontaneous polarization which may act as local electric field to align the trans-gauche ('TGTG') conformation into all-trans ('TTTT') conformation (β phases) of the PVDF molecule chains.

The SEM images (Fig. 2) show the morphologies of BST nanoparticles and BST-P(VDF-TrFE) nanocomposites. It can be found that the BST nanoparticles used in fabrication of the nanocomposites have round shapes and their sizes are typically below 30 nm. Fig. 2(c) and 2(d) show the cross-sectional and surface views of BST-P(VDF-TrFE) nanocomposites after the addition of BST, respectively, in comparison with the cross-sectional view of P(VDF-TrFE) shown in Fig. 2(b). The BST nanoparticles are found to homogeneously disperse in the P(VDF-TrFE) matrix.

Conventional DSC and temperature-modulated DSC (TMDSC) analyses on pristine P(VDF-TrFE) and BST-P(VDF-TrFE) nanocomposite are shown in Fig. 3. The linear heating rate is 3 °C/min. For $Ba_{0.75}Sr_{0.25}TiO_3$ ceramic the phase transition from tetragonal to cubic phases (FE-to-PE transition) occurs at around 45 °C [7]. Because the content of BST is low (26 wt%) and the latent heat involved in the FE-to-PE transition of $Ba_{0.75}Sr_{0.25}TiO_3$ is small, the heat flow and specific heat of P(VDF-TrFE) containing BST nanoparticles do not show peaks around 45 °C. The

addition of BST nanoparticles seems to make the FE-to-PE transition at around 62 °C in the P(VDF-TrFE) more diffusive, as shown in the endothermal peaks of heat flows and the peaks of reversible specific heat of the samples in Fig. 3(a) and 3(b)(c), respectively. The diffuse FE-to-PE transition in P(VDF-TrFE) matrix is attributed to the formation of nano-regions of α and β phases due to the presences of second-phase BST nano-particles. The peak of reversible specific heat slightly shifts to higher temperature with decreasing modulation period, showing that the FE-to-PE transition of P(VDF-TrFE) is of relaxor type. On the contrary, although the FE-to-PE transition of BST-P(VDF-TrFE) is more diffusive, the peak of reversible specific heat does not shift with modulation period. These TMDSC results thus suggest that the BST nano-fillers indeed enhance the ordering of nano-regions of α and β phases in the P(VDF-TrFE) matrix.

3.2 Ferroelectric and electro-carloric properties of the nanocomposites

The ferroelectric properties of P(VDF-TrFE) and BST-P(VDF-TrFE) films with the same dimensions are determined from the P-E loops, as shown in Fig. 4. The pristine P(VDF-TrFE) without any electric poling or mechanical stretching exhibits a weak remnant polarization much smaller than 1 μC/cm^2. However, the BST-P(VDF-TrFE) nanocomposite has typical P-E hysteresis loop with significant remnant polarization, as shown in Fig. 4(a). The results are consistent with those from XRD characterization that the α phase is dominant in the pristine P(VDF-TrFE) and the addition of BST nanoparticles results in the significantly increased content of polar β phase in the nanocomposite. Basically, it is difficult to induce large

polarization in the P(VDF-TrFE) under an electric field below 1 MV/cm. In the BST-P(VDF-TrFE) nanocomoposite, the relatively large polarization can be produced by the much lower electric field (<0.5 MV/cm). Under the same electric field, the polarization of BST-P(VDF-TrFE) is even better than that of P(VDF-TrFE) well processed by electric poling [8]. The enhanced polarization in the nanocomposite suggests that the BST nano-fillers could contribute to the ordering of dipoles of molecule groups such as $–CF_2$ and $–CH_2$ in PVDF.

Fig. 4(b) shows the P-E loops of BST-P(VDF-TrFE) at various temperatures and the saturation polarization is found to decrease with increasing temperature, indicating typical pyroelectric behaviors of ferroelectrics which result in the ECE. Fig. 5(a) and 5(b) illustrate the polarization changing with temperature for pristine P(VDF-TrFE) and BST-P(VDF-TrFE) nanocomposite, respectively. For pristine P(VDF-TrFE), the pyroelectric coefficient $(\partial D/\partial T)_E$ or $(\partial P/\partial T)_E$ is typically small and decreases with increasing applied electric field. BST-P(VDF-TrFE) has much larger pyroelectric coefficient which even increases with increasing applied electric field up to 600 kV/cm. Therefore the ECE of pristine P(VDF-TrFE) should be very weak while that of the nanocomposite is much larger.

The ECE is characterized by the entropy change (ΔS) or the refrigeration temperature change (ΔT) calculated by the thermodynamic Maxwell's equations, as follows:

$$\Delta S = \int_{E1}^{E2} \left(\frac{\partial D}{\partial T}\right)_E dE \quad , \qquad 1(a)$$

$$\Delta T = -\frac{T}{\rho C} \int_{E1}^{E2} \left(\frac{\partial D}{\partial T}\right)_E dE \ , \qquad 1(b)$$

where ρ is the density and C is specific heat capacity; D and P are electric displacement and polarization of the ferroelectrics, respectively; E_1 and E_2 are the lower and upper limits of the applied fields, respectively. Fig. 6 shows the ΔT in BST-P(VDF-TrFE) nanocomposite at different temperatures and E_2. It can be found that the largest ECE for nanocomposite occurs between 75 °C and 80 °C close to the Curie temperature of P(VDF-TrFE), and the ΔT is 2.5 °C when E_2 is 0.6 MV/cm and E_1 is 0.2 MV/cm. Thus the EC strength, i.e., $\alpha=\Delta T/(E_2-E_1)=6.25$ K·cm·MV^{-1}, is much larger than any ferroelectric co-polymer under the same conditions of applied electric fields. Based on the pyroelectric properties of the nanocomposite that $(\partial P/\partial T)_E$ increases with increasing applied field, it is expected that BST-P(VDF-TrFE) nanocomposite with a thickness lower than 1 μm could have the EC strength compatible with those of lead-free or lead-based ceramic thin films. Table 1 lists the EC temperature change and EC strength of other lead-free ferroelectrics [1,5,21-27] and the BST-P(VDF-TrFE) nanocomposite studied in this work.

Since the maximum ΔT occurs at a temperature (75 °C) well above the Curie temperature (45 °C) of BST, the ECE of the nanocomposite is dominated mainly by that of P(VDF-TrFE) matrix. On the other hand, the enhanced ECE of P(VDF-TrFE) compared with that of pristine P(VDF-TrFE) could be associated with the interface between the BST and the copolymer.

3.3 Dynamical mechanical analyses on the effects of BST on the enhanced ECE

Although it is argued that there is a size-driven FE-to-PE transition in ferroelectric ceramic nano-particles with a diameter *d* below 100 nm, the results

described in Sec.4.1 and Sec.4.2 show that BST nano-particles with D<30 nm still possess ferroelectricity. The increased content of polar crystalline β phase in the nanocomposite due to the addition of BST nanoparticles is not relate with the cross-linked VDF and TrFE since chemical reaction between BST and VDF or TrFE does not likely occur, while the BST nanoparticles with spontaneous polarization may act as local electric field strong enough to align the 'TGTG' conformation into 'TTTT' conformation of the PVDF molecule chains.

Low-frequency mechanical relaxation of nanocomposite close to the Curie temperature of P(VDF-TrFE) is employed to analyze the effect of BST nanoparticles on FE-to-PE transition in the P(VDF-TrFE) matrix. Fig. 7(a) shows the mechanical loss (Q^{-1}) and storage modulus of pristine P(VDF-TrFE) where the FE-to-PE transition can be identified by a peak in the Q^{-1} curve and a significant kink in the storage modulus curve. Unlike those in ceramic ferroelectrics which are of ferro-elastic type in the mechanical relaxation process, the FE-to-PE transition in pristine P(VDF-TrFE) is accompanied by the typical glassy behaviors of polar domain relaxation characterized by the Vogel-Fulcher-Tammann (VFT) relation as follows,

$$f = f_0 e^{-E_a/k_B(T-T_f)} \quad , \qquad (2)$$

where f is the test frequency and f_0 is the attempt frequency; E_a denotes the apparent activation energy for the polar domains and k_B is the Boltzmann constant. T_f represents the Kauzmann temperature or static freezing temperature which is far below the Curie temperature, assuming the polar domains are in a glassy state. Previous dielectric relaxation studies on P(VDF-TrFE) have revealed that VFT relation should be applied to the relaxation of polar domains in P(VDF-TrFE) and the

T_f is about 20 °C [30]. Using the same T_f, the mechanical relaxation in this work thus predicts an E_a of 0.11 eV, as shown in Fig. 8. The apparent activation energy obtained from the mechanical relaxation is consistent with that [20,30] determined by dielectric relaxation, demonstrating that the mechanical relaxation is effective in characterizing the structural and ferroelectric properties of the co-polymer.

The addition of BST nanoparticles significantly shifts the Q^{-1} peak to a higher temperature under the same testing frequency, as shown in Fig. 7(b). The apparent activation energy E_a of the polar domains in BST-P(VDF-TrFE) is determined to be 0.21 eV using Eq. (2), as shown in Fig. 8. The much larger activation energy compared with that of the pristine P(VDF-TrFE) implies that the BST nano-fillers stabilize the polar domains in the P(VDF-TrFE) matrix and reduce the glassy behaviors of polar domain relaxation, resulting in the enhanced polarization of BST-P(VDF-TrFE).

Most interestingly, the storage modulus of BST-P(VDF-TrFE) nanocomposite shows a 'cusp', which is an important characteristic of ferro-elastic polar domains during the FE-to-PE transition in ceramics. The increased peak temperature and apparent activation energy of BST-P(VDF-TrFE) compared with those of P(VDF-TrFE) further support the conclusion we draw from the XRD results and ferroelectric measurements that the BST addition should improve the content of ordered β phase. Furthermore, the existence of a 'cusp' or the soft-mode behavior in the elastic modulus during the FE-to-PE transition in P(VDF-TrFE) with BST nano-fillers clearly indicates the important role of spontaneous polarization of BST

nanoparticles in enhancing the ferroelectric and pyroelectric properties of P(VDF-TrFE). Because the BST nano-fillers could reduce the glassy behaviors of polar domain relaxation, some portions of polar domains in the P(VDF-TrFE) matrix might become ferro-elastic, in consistent with those of conventional ferroelectrics.

3.4 Discussions on the enhanced ECE in P(VDF-TrFE) with BST nano-fillers

The results of XRD, DMA and in-direct measurement on ECE described above have revealed that the enhanced ECE of BST-P(VDF-TrFE) compared with that of pristine P(VDF-TrFE) could be associated with the interface between the BST and the copolymer. Although there are a lot of factors such as the sizes and contents of nanoparticles, chemical composites of the nanoparticle surface and the microstructure of BST-P(VDF-TrFE) that could affect the interface between the BST and the copolymer, the enhanced ECE of BST-P(VDF-TrFE) compared with that of pristine P(VDF-TrFE) is mainly caused by the local dielectric and ferroelectric properties near the interfaces.

Because of the difference in the dielectric constants between BST and copolymer, the local electric displacement in the matrix region near the BST surface is much larger than that in the matrix homogeneously induced by the applied electric field [28,29]. The larger electric field is applied on the nanocomposite, the stronger electric displacement D in the matrix region near the BST surfaces or the larger electric energy stored in the nanocomposite could occur. Such intensified D thus result in the increase of the pyroelectric coefficient with increasing applied field, as

shown in Fig. 5(b). Therefore the EC refrigeration effect $Q_{ref}=T\Delta S$ calculated by Eq. 1(a) for the nanocomposite is much larger than that of pristine P(VDF-TrFE).

The effects of interfaces between the BST nanoparticles and the P(VDF-TrFE) matrix on the enhanced ECE in the nanocomposites can be elucidated by the principles of refrigeration. As pointed out by the Clausius statement in thermodynamics, work is required to generate refrigeration with an efficiency defined as the ratio of Q_{ref} to the work input. The refrigeration efficiency of nanocomposite should not be less than that of pristine P(VDF-TrFE) since the BST nano-fillers enhance the content of ferroelectric refrigerant. Under the same conditions of applied field, larger electric energy stored or the work input in the nanocomposite should lead to higher Q_{ref} or ΔT.

The effect of nanoparticle size *d* on the enhanced ECE in BST-P(VDF-TrFE) should be also considered. With the same content in the nanocomposite, larger BST nano-fillers possess lower surface-to-volume ratio. The electric energy stored and the content of ferroelectric polar phase induced by the BST nano-fillers in BST-P(VDF-TrFE) could decrease with increasing *d*. The quantitative relation between ΔT and *d* deserves systematic investigations.

Based on the aforementioned mechanisms of enhanced ECE in BST-P(VDF-TrFE), the chemical composition of the nanoparticle surface is one of the significant factors that affect the ECE of the nanocomposites. Chemical heterogeneity of BST nanoparticles may be introduced by functional groups on their surface or core-shell structures of the nanoparticles. With appropriate chemical

modification on their surface, the BST nano-fillers may have improved adhesion with the copolymer matrix, resulting in the increased electric breakdown field. However the chemically modified surfaces of BST would reduce the electric energy stored and the content of ferroelectric polar phase induced by the ferroelectric BST nano-fillers in BST-P(VDF-TrFE). Therefore under the same applied field, the ECE in P(VDF-TrFE) filled with nanoparticles with chemically modified surface should be less than that in BST-P(VDF-TrFE).

The microstructures of BST-P(VDF-TrFE) are mainly determined by the conditions of synthesis and post-processing of the nanocomposites such as mechanical stretching and electric polling. Nevertheless the content of BST nano-fillers is much easy to be controlled. As a results of larger interfacial regions between the BST nanoparticles and the copolymer matrix, the ECE of BST-P(VDF-TrFE) is enhanced with higher BST content. On the other hand, the electric breakdown field of the nanocomposite decreases with increasing BST content. Therefore an appropriate BST content corresponding to a maximum ECE is expected, which should be smaller than the percolating threshold of a composite system, e.g., 31% volume faction of spherical particles arranged at the cubic lattice sites in the matrix.

4. Conclusions

BST nanoparticles with a mean size below 30 nm are synthesized by a facile hydrothermal method for the fabrication of BST-P(VDF-TrFE) nanocomposites. Significantly enhanced ECE is observed in this lead-free ferroelectric nanocomposite

compared with that of pristine P(VDF-TrFE). The enhanced ECE is related with the increased content of β phase in P(VDF-TrFE) matrix due to the local electric fields imposed by the spontaneous polarizations of BST nanoparticles, and the enhanced electric energy stored in the co-polymer matrix region near the nanoparticle surfaces under applied electric fields. The nanocomposites reported in this study are flexible and easy to process and have a giant EC strength compatible to those of any other lead-free or lead based ferroelectrics. The underlying mechanisms of the enhanced ECE of the BST-P(VDF-TrFE) revealed in this study provide useful information for engineering ferroelectric polymer-ceramic nanoparticle nanocomposites with giant ECE, which are ideal refrigerants for environmental-friendly solid-state refrigeration.

Acknowledgements

The authors are grateful for the supports provided by the National Natural Science Foundation of China (No. U1304203), the Science and Technology Innovation Commission of Shenzhen, and the Program for Eastern Scholar at Shanghai Institutions of Higher Learning.

References

[1] S.G. Lu, Q.M. Zhang, Electrocaloric Materials for Solid State Refrigeration, Adv. Mater. (Weinheim, Ger.), 2009, 21, 1983-1987.

[2] X. Moya, S. Kar-Narayan, N.D. Mathur, Caloric Materials Near Ferroic Phase transitions, Nat. Mater., 2014, 13, 439-450.

[3] A.S. Mischenko, Q. Zhang, J.F. Scott, R.W. Whatmore, N.D. Mathur, Giant Electrocaloric Effect in Thin‐film $PbZr_{0.95}Ti_{0.05}O_3$, Science (Washington, DC, U.S.), 2006, 311, 1270–1271.

[4] Y. Bai, G.P. Zheng, S.Q. Shi, Direct Measurement of Giant Electrocaloric Effect in $BaTiO_3$ Multilayer Thick Film Structure beyond Theoretical Prediction, Appl. Phys. Lett., 2010, 96, 192902.

[5] L. Wang, J. Wang, B. Li, X. Zhong, F. Wang, H. Song, Y. Zeng, D. Huang, Y. Zhou, Enhanced Room Temperature Electrocaloric Effect in Barium Titanate Thin Films with Diffuse Phase Transtion, RSC Adv., 2014, 4, 21826–21829.

[6] X. Moya, E. Stern-Taulats, S. Crossley, D. Gonzalez-Alonso, S. Kar-Narayan, A. Planes, L. Manosa, N.D. Mathur, Giant Electrocaloric Strength in Single-Crystal $BaTiO_3$, Adv. Mater., 2013, 25, 1360-1365.

[7] K. Ding, G.P. Zheng, Scaling for the Refrigeration Effects in Lead-free Barium Titanate based Ferroelectric Ceramics, J. Electroceramics, 2014, 32, 169-174.

[8] B. Neese, B. Chu, S.G. Lu, Y. Wang, E. Furman, Q.M. Zhang, Large Electrocaloric Effect in Ferroelectric Polymers Near Room Temperature, Science (Washington, DC, U.S.), 2008, 321, 821–823.

[9] Y. Bai, G.P. Zheng, K. Ding, S.Q. Shi, L.J. Qiao, The Giant Electro-caloric Effect and Cooling Power of $BaTiO_3$ Thick Films, J. of Appl. Phys., 2011, 110, 094103.

[10] S.G. Lu, B. Rozic, Z. Kutnjiak, Q.M. Zhang, Electrocaloric Effect in Ferroelectric P(VDF-TrFE) Copolymer, Integr. Ferroelectrics, 2011, 125, 176-185.

[11] G. Zhang, Q. Li, H. Gu, S. Jiang, K. Han, M. R. Gadinski, M. A. Haque, Q. Zhang and Q. Wang, Ferroelectric Polymer Nanocomposites for Room-Temperature Electrocaloric Refrigeration , Adv. Mater. 2015, 27, 1450–1454

[12] Q. Li, G. Zhang, X. Zhang, S. Jiang, Y. Zeng and Q. Wang, Relaxor Ferroelectric-Based Electrocaloric Polymer Nanocomposites with a Broad Operating Temperature Range and High Cooling Energy, Adv. Mater. 2015, 27, 2236–2241

[13] G.T. Davis, T. Furukawa, A.J. Lovinger, M.G. Broadhurst, Structural and Dielectric Investigation on the Nature of the Transition in a Copolymer of Vinylidene Fluride and Trifluoroethylene (52/48%), Macromolecules, 1982, 15, 329-333.

[14] T. Hu, H. Jantunen, A. Uusimaki, S. Leppavuori, BST Powder with Sol-gel Process in Tape Casting and Firing, J. Euro. Ceram. Soc., 2004, 24, 1111–1116.

[15] K.A. Razak, A. Asadov, W. Cao, Properties of BST Ceramics Prepared by High Temperature Hydrothermal Process, Ceram. Inter., 2007, 33, 1495.

[16] A. Ioachim, F. Vasiliu, M.I. Toacsan, L. Nedelcu, M.G. Banciu, H.V. Alexandru, G. Stroica, Dielectric and Morphological Studies of BST Ferroelectric Ceramic, J. Optoelectron. and Adv. Mater., 2007, 9, 1576-1581.

[17] J.E. Mancilla, J.N. Rivera, C.A. Hernandez, M.G. Zapata, On the Dielectric and Ferroelectric Properties of $Ba_{0.75}Sr_{0.25}TiO_3$ Thin Film Deposited by RF Sputtering, J. Austra. Ceram. Soc., 2012, 48, 223-226.

[18] M.C. Gust, L.A. Momoda, N.D. Evans, M.L. Mecartney, Crystallization of Sol-Gel-Derived Barium Strontium Titanate Thin Films, J. Am. Ceram. Soc., 2001, 84, 1087-1092.

[19] S. Ueno, K. Nakashima, Y. Sakamoto, S. Wada, Synthesis of Silver-Strontium Titanate Hybrid Nanoparticles by Sol-Gel-Hydrothermal Method, Nanomaterials, 2015, 5, 386-397.

[20] G.T. Davis, T. Furukawa, A.J. Lovinger, M.G. Broadhurst, Structural and Dielectric Investigation on the Nature of the Transition in a Copolymer Vinylidene Fluoride and Trifluoroethylene (52/48 mol %), Macromolecules, 1982, 15, 329-333.

[21] H. Kaddoussi, Y. Gagou, A. Lahmar, J. Belhadi, B. Allouche, J.-L.Dellis, M. Courty, H. Khemakhem, M. ElMarssi, Room Temperature Electro-caloric Effect in Lead-free $Ba(Zr_{0.1}Ti_{0.9})_{1-x}Sn_xO_3$ (x=0, x=0.075) Ceramics, Solid State Comm., 2015, 201, 64–67.

[22] H. Chen, T. L. Ren, X. M. Wu, Y. Yang and L. T. Liu, Giant Electrocaloric Effect in Lead-free Thin Film of Strontium Bismuth Tantalite, Appl.Phys. Lett., 2009, 94, 182902.

[23] X. Y. Li, X. S. Qian, S. G. Lu, J. P. Cheng, Z. Fang and Q. M. Zhang, Tunable Temperature Dependence of Electrocaloric Effect in Ferroelectric Relaxor Poly(vinylidene fluoride-trifluoroethylene-chlorofluoroethylene Terpolymer, Appl. Phys. Lett., 2011, 99, 052907.

[24] Y. Bai, K. Ding, G. P. Zheng, S.Q. Shi, L. J. Qiao, Entropy-change Measurement of Electrocaloric Effect of $BaTiO_3$ Single Crystal, Phys. Stat. Solidi A, 2012, 209, 941

[25] K. Ding, G. P. Zheng, Scaling for the Refrigeration Effects in Lead-free Barium Titanate Based Ferroelectric Ceramics, J. Electroceramics, 2014, 32, 169.

[26] X. C. Zheng, G. P. Zheng, Z. Lin, Z.Y. Jiang, Electrocaloric Behaviors of BNT-BT Ceramics, J. Electroceramics, 2012, 28, 20.

[27] X. C. Zheng, G. P. Zheng, Z. Lin, Z.Y. Jiang, Thermo-electrical Energy Conversions in Bi0.5Na0.5TiO3-BaTiO3 Thin Films Prepared by Sol-gel Method, Thin Solid Films, 2012, 522, 125.

[28] Y. Feng, W.L. Li, Y.F. Hou, Y. Yu, W.P. Cao, T.D. Zhang, W.D. Fei, Enhanced Dielectric Properties of PVDF-HFP/$BaTiO_3$-Nanowire Composites Induced by Interfacial Polarization and Wire-shape, J. Mater. Chem. C, 2015, 3, 1250-1260.

[29] M. Arbatti, X. Shan, Z. Cheng, Ceramic–Polymer Composites with High Dielectric Constant, Adv. Mater., 2007, 19, 1369-1372.

[30] V. Bharti, H.S. Xu, G. Shanthi, Q.M. Zhang, Polarization and Structural Properties of High-energy Electron Irradiated Poly(vinylidene fluoride-trifluoroethylene) Copolymer Films, J. Appl. Phys., 2000, 87, 452-460.

Figure captions:

Figure 1. (a) XRD patterns of BST, P(VDF-TrFE) and BST-P(VDF-TrFE) samples. (b) (110) peaks of β phases in P(VDF-TrFE) (dash dot line) and BST-P(VDF-TrFE) (dash line).

Figure 2. SEM micrographs of BST (a), cross sections of P(VDF-TrFE) (b) and BST-P(VDF-TrFE) (c), and surface of BST-P(VDF-TrFE).

Figure 3. Heat flows of P(VDF-TrFE) and BST-P(VDF-TrFE) (a); reversible specific heats of P(VDF-TrFE) (b) and BST-P(VDF-TrFE) (c) at various periods t of modulated temperatures.

Figure 4. (a) P-E loops of P(VDF-TrFE) and BST-P(VDF-TrFE) at 24 ^{o}C. (b) P-E loops of BST-P(VDF-TrFE) at various temperatures.

Figure 5. Temperature-dependent polarization of P(VDF-TrFE) (a) and BST-P(VDF-TrFE) (b) under various maximum applied electric fields.

Figure 6. EC temperature changes of the nanocomposites.

Figure 7. Mechanical loss (Q^{-1}) and storage modulus of P(VDF-TrFE) (a) and BST-P(VDF-TrFE) (b).

Figure 8. Determination of the activation energies of FE-to-PE transitions in P(VDF-TrFE) and BST-P(VDF-TrFE) using Eq. (2)

Table 1. EC temperature change ΔT_{max} and EC strength α of lead-free ferroelectrics with different structures (Single crystal: SG; bulk: BK; thin film: TNF; thick film: TKF and multilayer: ML) and BST-P(VDF-TrFE) nanocomposite under the maximum applied field E_{max}.

	Structures	E_{max} (kV/cm)	ΔT_{max} (K)	α (K·cm/MV)	Ref.
$BaTiO_3$	SG	10	1.6	16	[24]
$BaTiO_3$	TNF	216.7	0.46	2	[5]
$BaTiO_3$	ML	800	7.4	9	[25]
$Ba_{1-x}Sr_xTiO_3$	BK	15	0.23	15	[25]
$(1-x)Bi_{0.5}Na_{0.5}TiO_3$-$xBaTiO_3$	BK	60	2.1	35	[26]
$(1-x)Bi_{0.5}Na_{0.5}TiO_3$-$xBaTiO_3$	TNF	862	3	3	[27]
$Ba(Zr_{0.1}Ti_{0.9})O_3$	TKF	8.7	0.2	23	[21]
$SrBiTa_2O_9$	TNF	600	4.93	8	[22]
P(VDF-TrFE)	TNF	1200-3000	12-21	6-10	[1]
P(VDF-TrFE-CFE)	TNF	1500	15.7	10.5	[23]
BST- P(VDF-TrFE)	TKF	600	2.5	6.25	This work

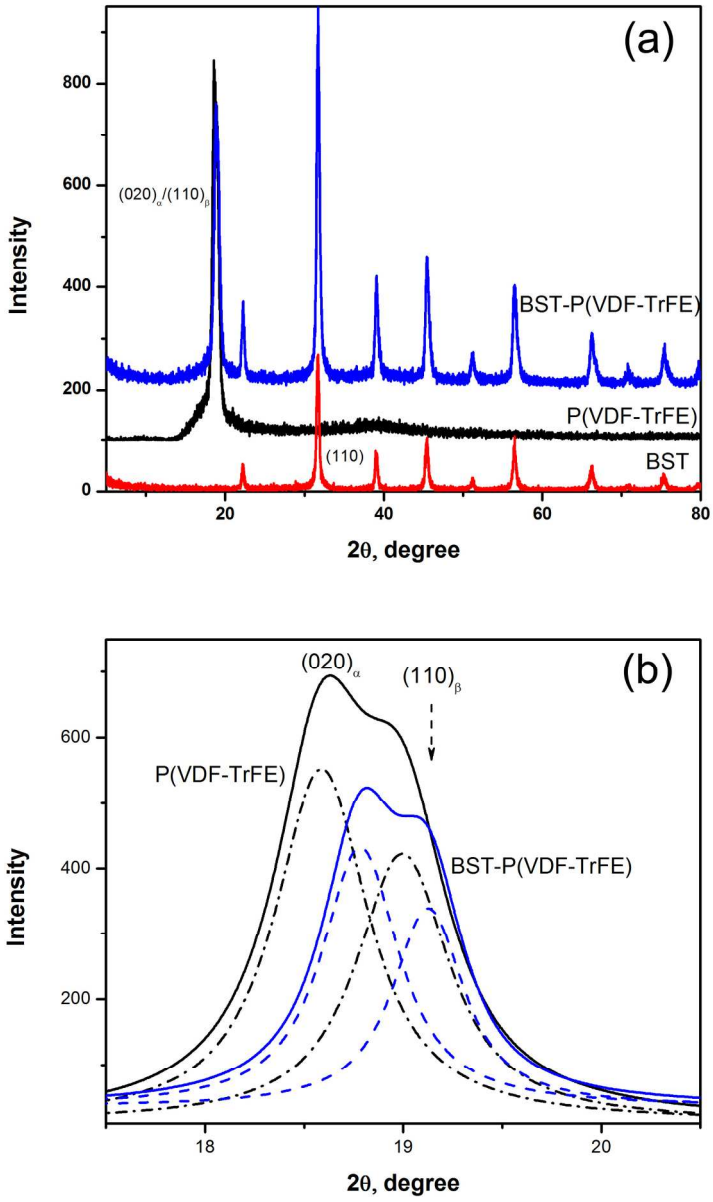

139x233mm (300 x 300 DPI)

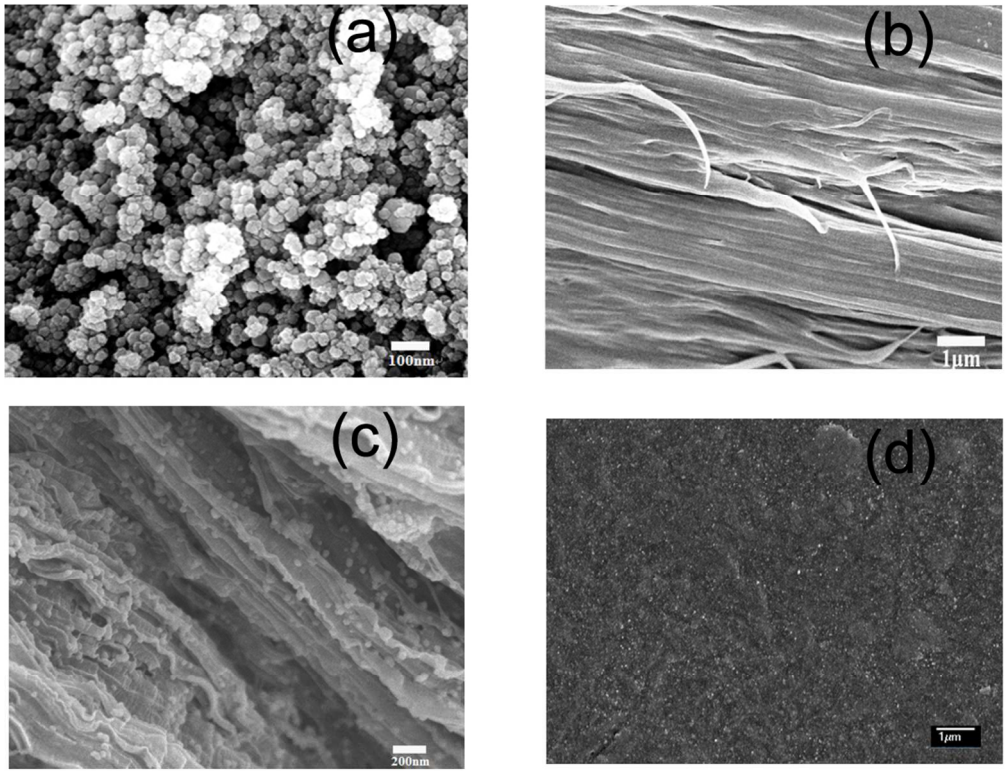

423x324mm (72 x 72 DPI)

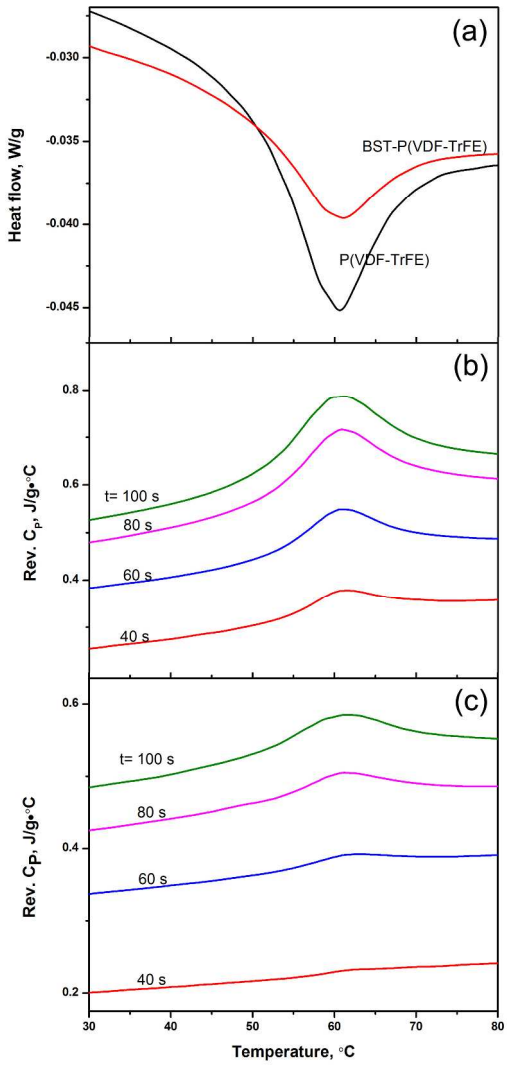

203x458mm (300 x 300 DPI)

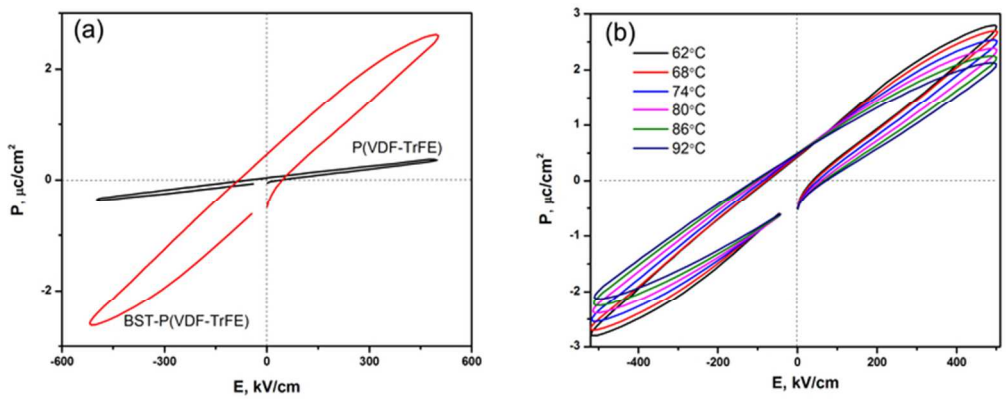

66x26mm (300 x 300 DPI)

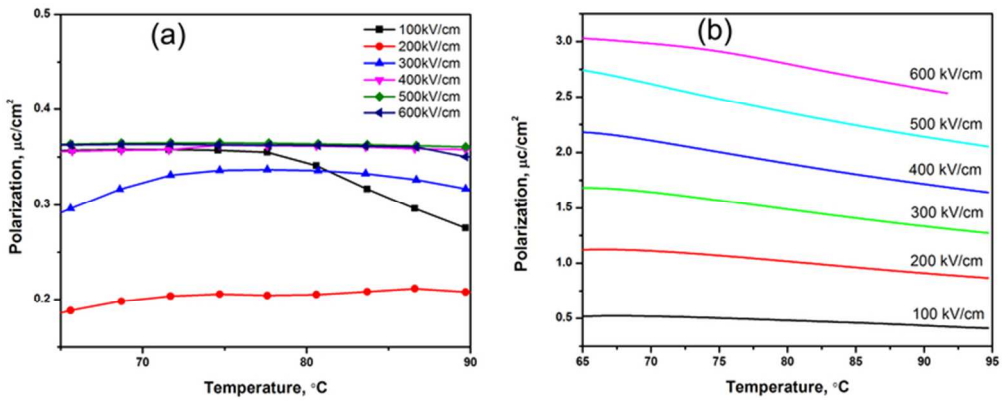

67x26mm (300 x 300 DPI)

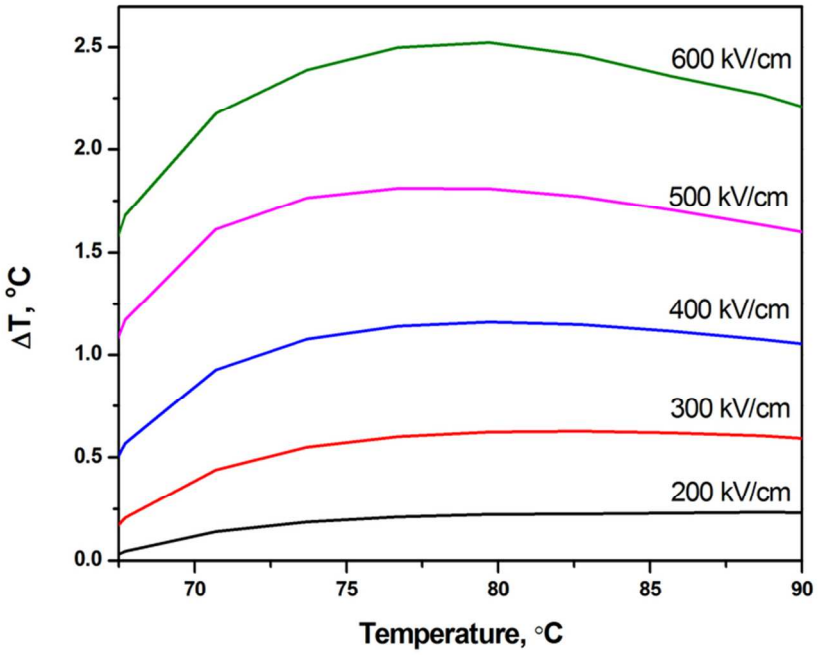

78x60mm (300 x 300 DPI)

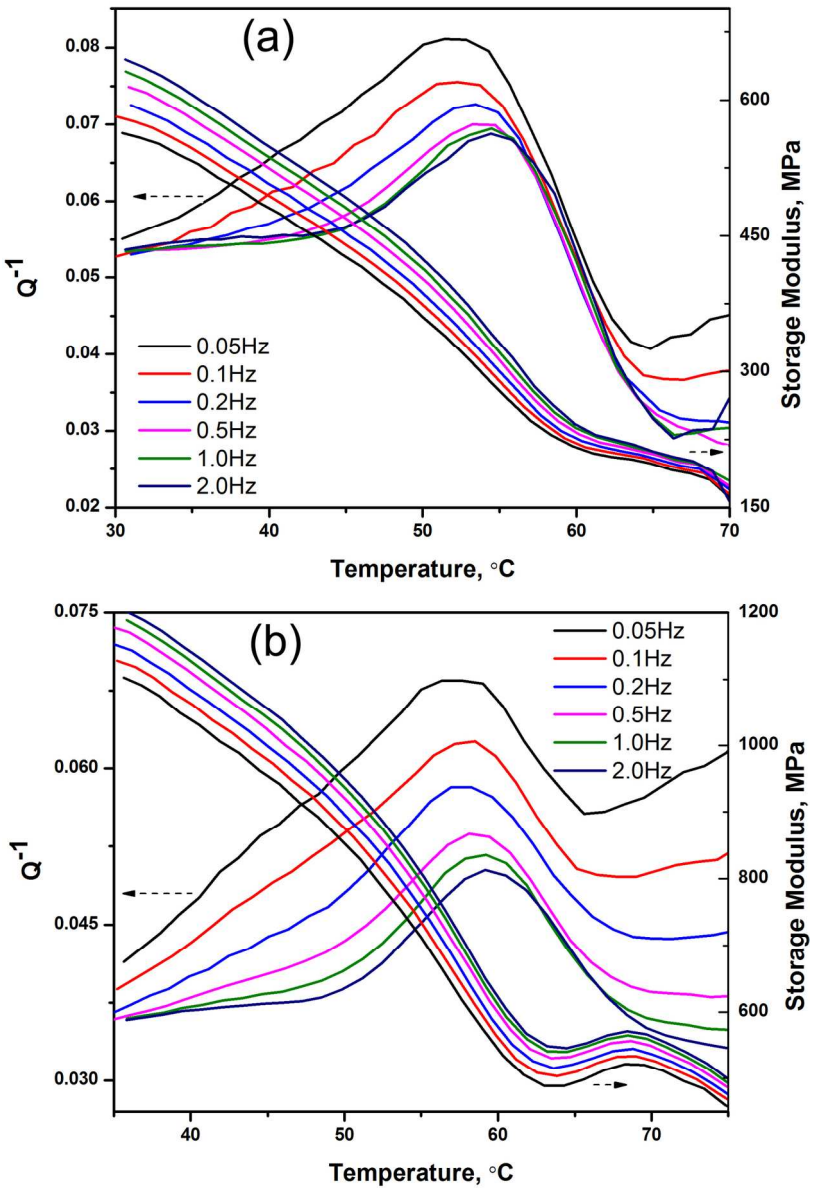

135x201mm (300 x 300 DPI)

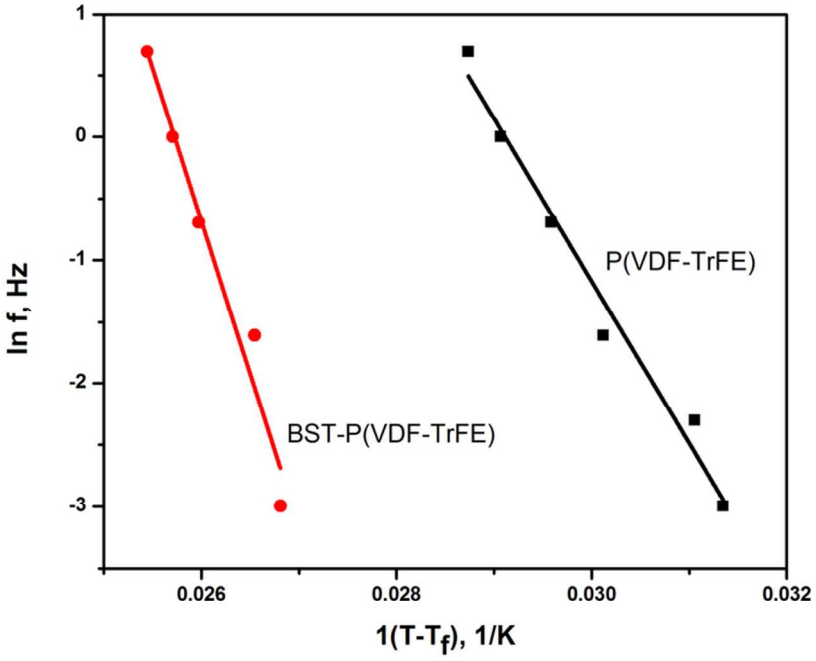

78x60mm (300 x 300 DPI)